Isotopic filtering reveals high sensitivity of planktic calcifiers to Paleocene–Eocene thermal maximum warming and acidification

Brittany N. Hupp[a,1], D. Clay Kelly[a], and John W. Williams[b]

[a]Department of Geoscience, University of Wisconsin–Madison, Madison, WI 53706; and [b]Department of Geography and Center for Climatic Research, University of Wisconsin–Madison, Madison, WI 53706

Edited by Nils Chr. Stenseth, Centre for Ecological and Evolutionary Synthesis, Department of Biosciences, Universitetet i Oslo, Oslo, Norway; received August 23, 2021; accepted January 19, 2022

Ocean warming and acidification driven by anthropogenic carbon emissions pose an existential threat to marine calcifying communities. A similar perturbation to global carbon cycling and ocean chemistry occurred ∼56 Ma during the Paleocene–Eocene thermal maximum (PETM), but microfossil records of the marine biotic response are distorted by sediment mixing. Here, we use the carbon isotope excursion marking the PETM to distinguish planktic foraminifer shells calcified during the PETM from those calcified prior to the event and then isotopically filter anachronous specimens from the PETM microfossil assemblages. We find that nearly one-half of foraminifer shells in a deep-sea PETM record from the central Pacific (Ocean Drilling Program Site 865) are reworked contaminants. Contrary to previous interpretations, corrected assemblages reveal a transient but significant decrease in tropical planktic foraminifer diversity at this open-ocean site during the PETM. The decrease in local diversity was caused by extirpation of shallow- and deep-dwelling taxa as they underwent extratropical migrations in response to heat stress, with one prominent lineage showing signs of impaired calcification possibly due to ocean acidification. An absence of subbotinids in the corrected assemblages suggests that ocean deoxygenation may have rendered thermocline depths uninhabitable for some deeper-dwelling taxa. Latitudinal range shifts provided a rapid-response survival mechanism for tropical planktic foraminifers during the PETM, but the rapidity of ocean warming and acidification projected for the coming centuries will likely strain the adaptability of these resilient calcifiers.

global warming | PETM | planktic foraminifera | ocean acidification | sediment mixing

Unabated carbon emissions are projected to raise atmospheric carbon dioxide (CO_2) concentrations to levels (850 parts per million volume [ppm], shared socio-economic pathway [SSP]3-7.0) that have not existed on Earth for nearly 50 million y and increase global temperatures by ∼4 °C over the coming centuries (1, 2). Much of the carbon emitted over this timeframe will be absorbed by the oceans, lowering seawater pH and increasing the solubility of carbonate minerals such as calcite ($CaCO_3$) that many marine organisms use to build their shells and exoskeletons (3–5). Thus, the combined effects of ocean warming and acidification pose an existential threat to marine calcifying organisms (6), including various calcareous plankton that are foundational to the marine food web (7–9).

To better understand the biotic consequences of human-induced climate change, many researchers have turned their attention to geological records of past greenhouse climate states. One such global warming event, the Paleocene–Eocene thermal maximum (PETM), occurred 56 million y ago and is considered a natural analog for ocean warming and acidification driven by anthropogenic CO_2 emissions (10, 11). Geochemical records show that sea surface temperatures (SSTs) warmed by ∼4 to 5 °C globally during the PETM (12, 13) and that this transient (∼170 ka) warming was coupled to a sharp rise in atmospheric CO_2 levels and a sustained period of ocean acidification (14–16). A global hallmark of the PETM is a decrease in the carbon isotope ($\delta^{13}C$) compositions of inorganic and organic materials in both marine and terrestrial records (17, 18). This negative carbon isotope excursion (CIE) signals a geologically rapid (≤5 kyr) release of massive quantities of ^{13}C-depleted carbon into the ocean–atmosphere system (11, 19–21), making it a reliable chemostratigraphic marker for correlating marine and continental PETM records from various sites around the world. However, close examination of the CIE signature in deep-sea sedimentary records has demonstrated that pelagic PETM records are often distorted by such preservation biases as carbonate dissolution, diagenesis, and sediment mixing (11, 14, 22, 23).

Of the aforementioned taphonomic processes, sediment mixing is arguably the most underappreciated impediment to achieving a clear understanding of the impacts that PETM warming and ocean acidification had on marine calcifiers. The marine microfossil record provides one of our best insights into past oceanic and biotic change, yet ocean currents and the burrowing activities of benthic organisms (bioturbation) blend anachronous microfossils into aggregate assemblages before they are incorporated into the deep-sea sedimentary archive (24). Vertical sediment mixing typically homogenizes surficial

Significance

Human-induced carbon emissions are causing global temperatures to rise and oceans to acidify. To understand how these rapid perturbations affect marine calcifying communities, we investigate a similar event in Earth's geologic past, the Paleocene–Eocene thermal maximum (PETM). We introduce a method, isotopic filtering, to mitigate the time-averaging effects of sediment mixing on deep-sea microfossil records. Contrary to previous studies, we find that tropical planktic foraminifers in the central Pacific ocean were adversely affected by PETM conditions, as evidenced by a decrease in local diversity, extratropical migration, and impaired calcification. While these species survived the PETM through migration to cooler waters, it is unclear whether marine calcifiers can withstand the rapid changes our oceans are experiencing today.

Author contributions: B.N.H. and D.C.K. designed research; B.N.H. performed research; B.N.H., D.C.K., and J.W.W. analyzed data; and B.N.H., D.C.K., and J.W.W. wrote the paper.

The authors declare no competing interest.

This article is a PNAS Direct Submission.

See online for related content such as Commentaries.

[1]To whom correspondence may be addressed. Email: brittanynhupp@gmail.com.

This article contains supporting information online at http://www.pnas.org/lookup/suppl/doi:10.1073/pnas.2115561119/-/DCSupplemental.

Published February 22, 2022.

sediments on time scales of 1,000s to 10,000s of years in pelagic settings (25, 26), which can potentially mask transitory ecological responses to rapid ocean-climate change. Indeed, high-resolution $\delta^{13}C$ records show that PETM assemblages of planktic foraminifers are time-averaged mixtures of ^{13}C-enriched shells calcified prior to the CIE and ^{13}C-depleted shells calcified during the CIE (e.g., refs. 27–29). And as we shall show, failure to account for the commingling of pre-CIE and CIE microfossils has perpetuated a longstanding misconception that tropical planktic foraminifers diversified in open-ocean settings during the PETM (27, 30).

Here, we reconstruct the response of tropical planktic foraminifers to PETM conditions by deconvolving the effects of sediment mixing through isotopic filtering, where the $\delta^{13}C$ signatures of 548 individual planktic foraminifer shells are used to filter out reworked, pre-CIE specimens from a series of samples taken from within the CIE interval of the PETM record from Ocean Drilling Program (ODP) Site 865. Paleolatitude projections (31) place Site 865 within a few degrees of the equator during the late Paleocene (Fig. 1*A*), and foraminifer $\delta^{13}C$ records have established that two parallel PETM records were recovered at Site 865 (32), one from drill Hole B and another from nearby drill Hole C. A wealth of single-shell $\delta^{13}C$ data ($n = 235$) was compiled for the 865C section by previous studies [Kelly et al., 1996 (27) and 1998 (30)], which we expanded by conducting supplementary single-shell analyses ($n = 313$ this study) on additional species and specimens from the CIE interval of the same section. Analytical limitations necessitated the use of relatively large (>250 μm) specimens for single-shell $\delta^{13}C$ measurements. Still, we are able to constrain the proportions of reworked pre-CIE and in situ CIE specimens for the nine most abundant taxa (*SI Appendix*, Figs. S1 and S2). The relatively high $\delta^{13}C$ signatures (~4‰) of pre-CIE morozovellids and acarininids indicate that these taxa inhabited the ^{13}C-rich waters of the euphotic zone, while the lower $\delta^{13}C$ values (~2‰) of pre-CIE subbotinids indicate biocalcification within deeper, ^{13}C-depleted waters of the thermocline (33, 34) (Fig. 1*B*).

Removal of foraminifer shells for stable isotope analyses has biased the taxonomic composition of the 865C assemblages. As a result, point-counted census data (>250 μm size fraction) were compiled for a fresh set of correlative samples from the CIE interval of the nearby 865B section and corrected for sediment mixing using the per-taxon estimates of reworked shells in the 865C section (*Materials and Methods*). Several stratigraphic features permit close cross-correlation of samples between the 865B and 865C PETM sections. Parallel bulk-carbonate $\delta^{13}C$ records show that the early stages of the PETM, extending from the CIE onset to just above the CIE minimum where bulk-carbonate $\delta^{13}C$ values start to return to higher values, were recovered at both sites (Fig. 1 *C* and *D*). Furthermore, initial studies of the Site 865 PETM planktic foraminifer assemblages identified a suite of short-lived "excursion taxa" (*Morozovella allisonensis*, *Acarinina sibaiyaensis*, *Acarinina africana*) whose biostratigraphic ranges are confined to the CIE interval (27, 30). Parallel assemblage counts (>125 μm size fraction) show that the peak abundance of these marker taxa is captured by both PETM records (Fig. 1 *E* and *F*). Astronomical tuning of deep-sea PETM records indicates that

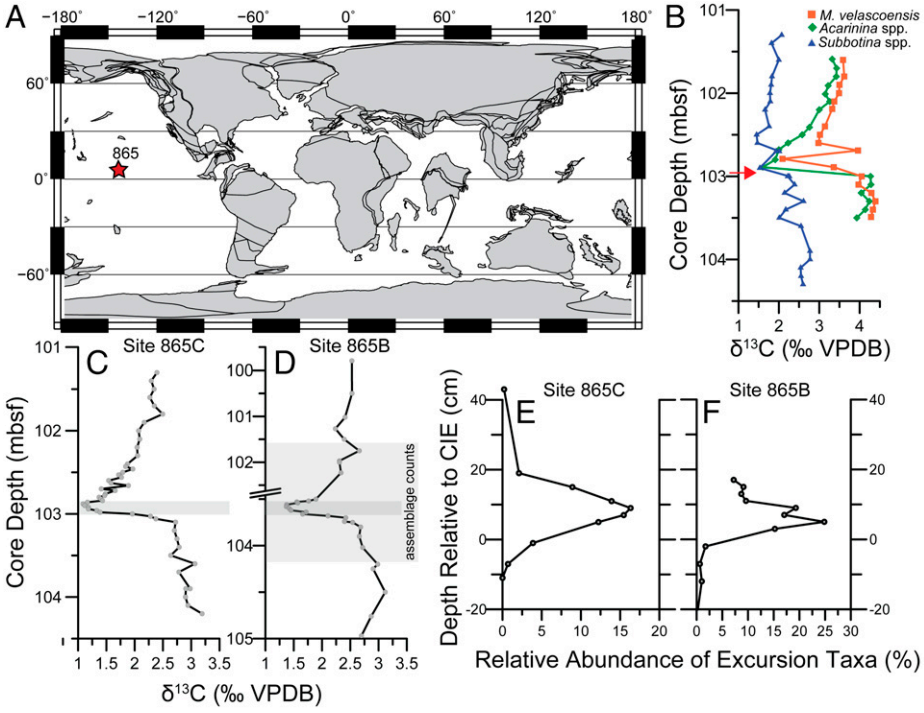

Fig. 1. Site 865 location and CIE marking the PETM. (*A*) Paleogeographic map showing tropical location of open-ocean Site 865 (red star) during the late Paleocene (source: Ocean Drilling Stratigraphic Network, odsn.de). (*B*) Planktic foraminifer carbon isotope ($\delta^{13}C$) records for the 865C section constructed with pooled, multishell samples of *M. velascoensis* (orange squares), *Acarinina* spp. (green diamonds), and *Subbotina* spp. (blue triangles) (32). The red arrow denotes stratigraphic position (meters below sea floor = mbsf) of the benthic foraminifer extinction event associated with CIE onset (32). (*C* and *D*) Bulk-carbonate $\delta^{13}C$ records of CIE in the 865C and 865B PETM sections, respectively. The break along vertical axis in panel *D* signifies a coring gap. The dark gray shading delimits the correlative lower CIE interval in the two PETM records. The light gray shading delimits the portion of 865B record sampled for planktic foraminifer assemblage counts. (*E* and *F*) Relative abundance curves showing acme of excursion marker taxa (*M. allisonensis, A. sibaiyaensis*, and *A. africana*) based on unfiltered census counts (>125 μm) for 865C and 865B PETM planktic foraminifer assemblages, respectively. Assemblage count data for the 865C PETM section taken from published literature (27). For comparative purposes, data shown are plotted relative (±cm) to stratigraphic level of CIE onset in bulk-carbonate $\delta^{13}C$ records, which was prescribed a reference depth of 0 cm.

this portion of the CIE spans the first 70 kyr of the event (26), thus the stratigraphies of the two Site 865 PETM records correlate well at millennial timescales (Fig. 1 *C–F*).

Results

Isotopic filtering reveals that nearly one-half (49.5%) of the 548 individual foraminifer shells analyzed are pre-CIE contaminants within the 865C PETM record (Fig. 2). The distributions of single-shell $\delta^{13}C$ values for the shallow-dwelling morozovellids and acarininids are distinctly bimodal (Fig. 2), indicating that these genera are distinguishable mixtures of reworked pre-CIE and in situ CIE shells. Conversely, the subbotinid $\delta^{13}C$ distribution is unimodal and centered on a pre-CIE value of ~2‰ (Figs. 1*B* and 2). This observation, in combination with the precipitous decline in subbotinid abundances in unfiltered census records over the CIE interval at Site 865 and other subtropical sites in the Pacific (35), indicates that all subbotinid shells are pre-CIE contaminants, as previously surmised (27, 30). Only 0.5% (n = 3) specimens register intermediate $\delta^{13}C$ values, which are believed to reflect either infilling of shells by diagenetic calcite (36) or the occasional downward mixing of shells from the overlying recovery stages of the CIE where $\delta^{13}C$ values begin to transition back toward higher post-PETM values (Fig. 1*C*).

Examination of single-shell $\delta^{13}C$ records for individual taxa reveals that the deep-dwelling subbotinids are not the only group represented by solely reworked, pre-CIE specimens (Fig. 3*A*). For instance, 100% of *Morozovella aequa*/*subbotinae* shells register pre-CIE values (Fig. 3*B*), as do the overwhelming majority of *Morozovella acuta*, *Morozovella velascoensis*, and *Acarinina soldadoensis* shells within the three lowermost samples (Fig. 3 *C–E*). We collectively refer to these five taxa as "Lazarus" taxa (37) because their single-shell $\delta^{13}C$ records demonstrate that they temporarily disappear over the CIE interval only to reappear higher in the Site 865 stratigraphy (Fig. 4*C*). By contrast, virtually none of the shells belonging to the shallow-dwelling species *Acarinina esnaensis* and *Acarinina esnehensis* register pre-CIE values within the CIE interval (Fig. 3 *F* and *G*). Thus, these two acarininid species are present before, during, and after the PETM, and so are called "holdover" taxa due to their uninterrupted occurrence. Finally, the "excursion" taxa (*M. allisonensis* and *A. sibaiyaensis*) have observed stratigraphic ranges restricted to the CIE interval at Site 865 (27) and their shells register almost exclusively CIE values (Fig. 3 *H* and *I*).

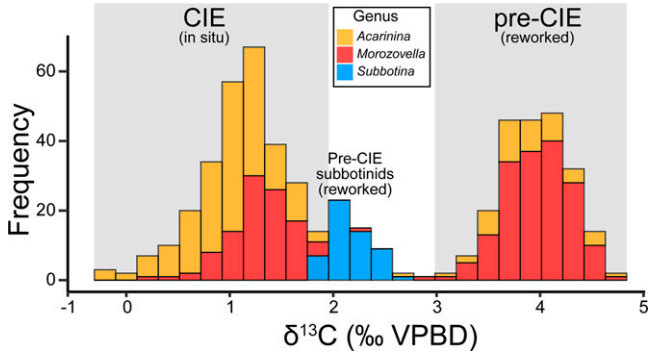

Fig. 2. Frequency distributions of single-shell $\delta^{13}C$ values for planktic foraminifers from the lower CIE of the Site 865C PETM record (n = 548). The bimodal distributions for shallow-dwelling genera *Morozovella* (n = 274) and *Acarinina* (n = 220) indicate that these taxa are mixtures of reworked, pre-CIE specimens with high $\delta^{13}C$ values and in situ CIE specimens with relatively low $\delta^{13}C$ values. The unimodal distribution of thermocline-dwelling genus *Subbotina* (n = 54) is centered on a pre-CIE value for this particular taxon, indicating that all subbotinids are reworked specimens.

Correcting for sediment mixing leads to a reversal of previously reported trends in local diversity (27, 30) and establishes that the transient excursion taxa were a major component of planktic foraminifer communities during peak PETM conditions (Fig. 4). Specifically, the uncorrected record yields an apparent increase in diversity, whereas the isotopically filtered record shows a sharp decrease in local diversity over the CIE interval (Fig. 4*A*). The relative abundances of the excursion taxa, *A. sibaiyaensis* and *M. allisonensis*, are greater than originally reported, accounting for nearly one-half (~45%) of the early CIE assemblages (Fig. 4*B*). Isotopic filtering also reaffirms that both the deep-dwelling *Subbotina* and shallow-dwelling *M. aequa*/*subbotinae* lineages disappear entirely over the main body of the CIE (Fig. 4*C*). Our data thus show that planktic foraminifer communities at Site 865 suffered an abrupt decrease in both taxonomic richness and evenness during the PETM, leaving a depauperate (oligotaxic) assemblage composed predominantly of acarininids (*A. esnaensis*, *A. esnehensis*, and *A. sibaiyaensis*) and the excursion morozovellid, *M. allisonensis* (Fig. 4*C*).

Discussion

PETM Extirpations: Tropical Exodus or Taphonomic Artifact? All taxa that disappear eventually reappear higher in the stratigraphy (Fig. 4*C*), indicating that no true extinctions are observed among planktic foraminifers at Site 865. Ocean acidification increased carbonate dissolution during the initial stages of the PETM (14, 38), and the dearth of intermediate values in our single-shell $\delta^{13}C$ dataset (Fig. 2) suggests that the transition from pre-CIE to CIE conditions was either extremely rapid or lost from the Site 865 record due to dissolution (36). Thus, the temporary disappearances of such Lazarus taxa (i.e., *Subbotina* spp., *M. aequa*/*subbotinae*, *M. velascoensis*, *M. acuta*, and *A. soldadoensis*) could be construed as a taphonomic artifact stemming from incomplete preservation (35). However, the presence of delicate *A. sibaiyaensis* and *M. allisonensis* shells contradicts a strong dissolution effect. Furthermore, the shells of some Lazarus taxa (*A. soldadoensis*, *M. aequa*/*subbotinae*, *M. velascoensis*, and *M. acuta*) are relatively resistant to dissolution (35, 39), which is inconsistent with a strong taphonomic overprint.

A more likely explanation is that the Lazarus taxa emigrated out of the study area toward cooler waters in response to extreme tropical warmth during the PETM. The collapse and subsequent reestablishment of *M. aequa*/*subbotinae* populations, which accounted for ~40 to 50% of the assemblages prior to the CIE, typifies such an extratropical migration (Fig. 4*C*). The hypothesis for extratropical migration by *M. aequa*/*subbotinae* is further supported by marked increases in their abundances throughout the circum-Antarctic region during the PETM (40)—increases that cannot be attributed to sediment mixing because these taxa were absent or present only in trace amounts in the southern high latitudes prior to the CIE. Our isotopically filtered census data thus suggest that some tropical planktic foraminifer taxa experienced both leading- and trailing-edge dynamics to their biogeographic ranges, where poleward range shifts were accompanied by local extirpations in the tropics. Similar range shifts are underway today (41).

Comparable spatiotemporal shifts in the biogeographic ranges of calcareous marine algae (coccolithophores) (42) and temperate continental vegetation (43) have been attributed to PETM warming, suggesting transient range shifts driven by transient climate change. In addition, transient disappearances of planktic foraminifers somewhat similar to those uncovered by this study have been observed in hemipelagic sections from the eastern (Tanzania) (44) and western (Nigeria) (45) margins of Africa, where complementary geochemical records indicate that tropical SSTs (>36 °C) likely exceeded the physiological temperature tolerances of many marine calcifiers. Likewise,

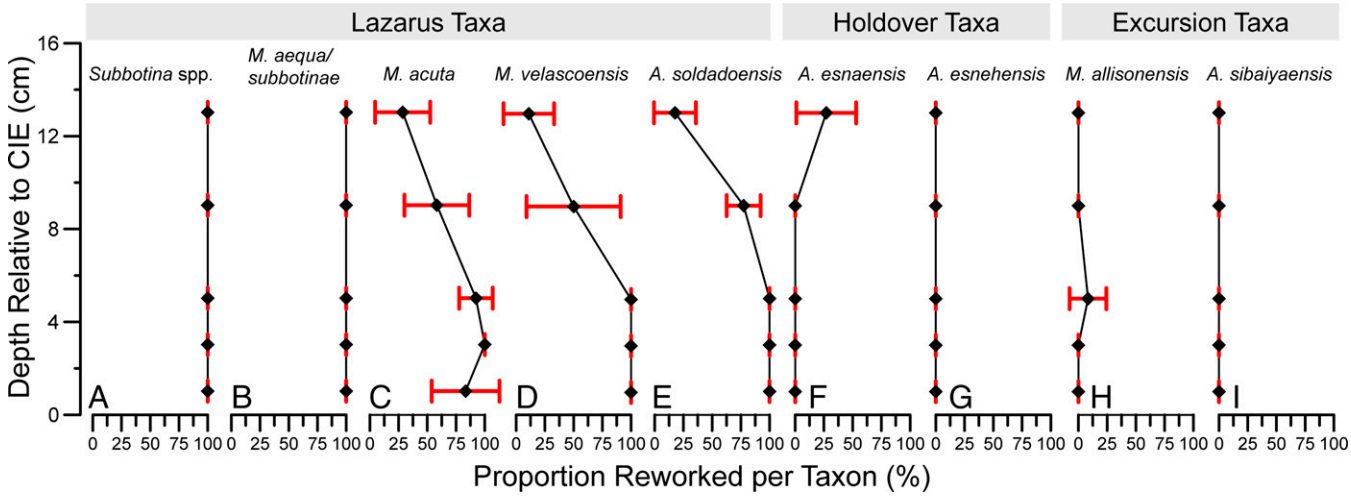

Fig. 3. Proportions of reworked specimens within the lower CIE of the 865C PETM section used to reconstruct population dynamics for individual planktic foraminifer taxa during the early stages of the CIE. (*A–E*) "Lazarus" taxa disappear over part or all of the early CIE only to subsequently reappear in the fossil record. (*F* and *G*) "Holdover" taxa occur continuously before, during, and after the PETM. (*H* and *I*) "Excursion" taxa occur almost exclusively during the early CIE. The red error bars delimit the 95% CI as determined by nonparametric bootstrapping (i.e., resampling) of proportions (1,000 iterations). The data are plotted relative (+cm) to stratigraphic level of CIE onset in Site 865C bulk-carbonate $\delta^{13}C$ record.

foraminifer $\delta^{18}O$ temperature records indicate that exceptionally warm SSTs (~33 °C) prevailed at Site 865 during the PETM (46). These observations suggest that the warming tropics became uninhabitable for some calcifying plankton, resulting in a tropical exodus of taxa as they emigrated out of the study area to escape extreme PETM warmth.

Site 865 shows that tropical pelagic ecosystems were profoundly perturbed during the PETM, yet planktic foraminifers did not suffer a major extinction event like that experienced by their benthic foraminifer counterparts, in which 40 to 60% of species were lost during the PETM (10, 47). Latitudinal range shifts among planktic foraminifers appear to have been temporary, with local communities returning to pre-event levels of richness and biodiversity following the PETM (Fig. 4*A*). The reestablishment of planktic foraminifer communities at Site 865 indicates that extratropical migration served as a rapid response for the survival of some taxa, which in turn allowed the expatriated taxa to quickly repopulate the tropics as PETM conditions waned. Hence, these results suggest a differential sensitivity of planktic and benthic foraminifers to ocean warming, perhaps because of a higher thermal heterogeneity in the surface ocean and/or potential for plankton to migrate more readily.

Synergistic Environmental Stressors. The tropical exodus of many planktic calcifiers indicates that heat stress was the primary driver for the temporary loss of diversity at low latitudes during the PETM (42, 44, 45), yet it is likely that attendant ocean acidification and deoxygenation also contributed to the planktic foraminifer response at Site 865. Stratigraphic unmixing by isotopic filtering shows that the taxa *M. acuta* and *M. velascoensis* were temporarily replaced by the excursion taxon, *M. allisonensis*, during the early stages of the CIE (Figs. 3 *C*, *D*, and *H* and 4*C*). The highly gradational morphologies of these taxa (30), in

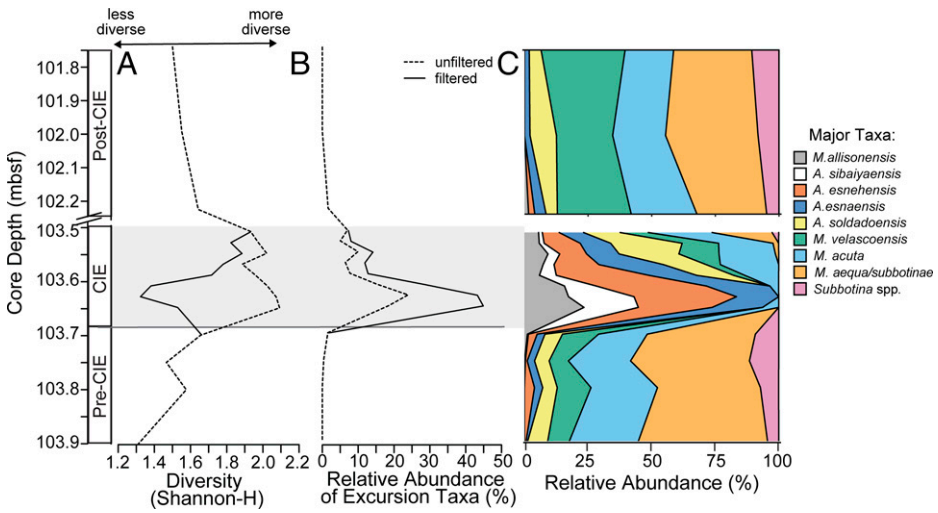

Fig. 4. Comparison of isotopically filtered and unfiltered planktic foraminifer assemblages from the 865B PETM section. Diversity metrics and relative abundances for the nine taxa sampled for single-shell stable isotope analyses (*Materials and Methods*). Comparisons include (*A*) diversity (Shannon-H) and (*B*) combined relative abundance of excursion taxa (*M. allisonensis* and *A. sibaiyaensis*). (*C*) Stacked-area plot showing changes in taxonomic composition and taxon relative abundances for isotopically filtered assemblages over the lower CIE in the 865B PETM section. The break along the vertical axis denotes coring gap in the 865B section (mbsf = meters below sea floor).

combination with the sequential order of their appearance and disappearance, suggest a plexus of forms in which the biconvex axially compressed shells of *M. allisonensis* represent deformed variants of the *M. acuta/velascoensis* lineage. We therefore view the brief appearance of the excursion taxon, *M. allisonensis*, as an ecophenotypic response to ocean acidification. Comparable morphological variation occurred among other calcareous plankton during the PETM, most notably the nannofossil genus *Discoaster* (48–50). As in the *M. velascoensis* lineage, increased morphological variability during the PETM gave rise to a continuum of *Discoaster* morphotypes, some of which are thought to be malformed ecophenotypes resulting from decreased calcite saturation (49, 51). Both culturing experiments (52) and field studies (9, 53–55) indicate that calcification in extant planktic foraminifers is impeded by lower pH and carbonate ion concentrations. Thus, the succession of phenotypes seen at Site 865, where *M. allisonensis* initially replaces *M. velascoensis* only to revert back to the antecedent *M. acuta/velascoensis* phenotype midway through the CIE interval, is consonant with the view that biocalcification and inorganic carbon production were inhibited during the PETM (49, 56), producing strong ecophenotypic responses.

Other researchers have suggested that thermal stress caused a breakdown in the symbiotic association between planktic foraminifers and photosynthetic microalgae (i.e., symbiont bleaching) during the PETM (57, 58). The photosynthetic activity of algal symbionts results in a positive relationship between $\delta^{13}C$ and shell size in photosymbiotic planktic foraminifers (59), and this $\delta^{13}C$-size relationship prevails in both acarininids and morozovellids (34, 60). However, size-segregated analyses of excursion taxa *M. allisonensis* and *A. sibaiyaensis* from Site 865 (30) indicate that these taxa retained the characteristic photosymbiotic $\delta^{13}C$-size relationship, and the $\delta^{13}C$ distributions for these two excursion taxa exhibit values similar to those registered by in situ CIE shells of *M. velascoensis*, *M. acuta*, and *A. soldadoensis*. Moreover, if symbiont bleaching occurred at Site 865, $\delta^{13}C$ signatures of large shells of symbiotic taxa would be expected to decrease by ~1‰ (59), while the statistical populations of reworked pre-CIE and in situ CIE specimens are separated by ~3‰ (Fig. 2). Hence, these observations do not fully rule out symbiont bleaching at the PETM but do suggest that its effect on our single-shell foraminifer $\delta^{13}C$ records is negligible.

Finally, ocean deoxygenation—driven by some combination of temperature solubility effects, changing ocean ventilation, increased nutrient input from continents (eutrophication), and/or methane hydrate destabilization—is thought to have contributed to the turnover in benthic foraminifer communities during the PETM (47, 61–64). There is now a large body of evidence to indicate that the oxygen content of seawater decreased globally during the PETM (65–68), including molecular biomarker (69) and barite sulfur isotope (70) records signaling the development of euxinic conditions within the water column. A warming-induced decrease in oxygen solubility and concomitant expansion of oxygen minimum zones (71) would have had dire consequences for planktic foraminifers with deeper depth ecologies such as the thermocline-dwelling subbotinids. Though paleoredox records indicate that oceanic bottom waters remained relatively well ventilated at Site 865 during the PETM (72), it does not preclude the possibility that an expanded oxygen minimum zone within the overlying water column contributed to the demise of local subbotinid populations by impinging upon their thermocline habitat.

Isotopic Filtering and Implications for the Future Health of Pelagic Calcifiers. This case study demonstrates how isotopic filtering can be used to unmix microfossil assemblages that have been blended by sediment mixing processes, thereby enhancing the fidelity of fossil records chronicling transitory biotic responses to past episodes of rapid biogeochemical and climate change. Here, isotopic filtering reveals a previously unrecognizable biotic crisis among tropical planktic foraminifer communities at Site 865, as signaled by an abrupt decrease in local diversity during the PETM. Though no true extinctions are observed (73), extreme PETM warmth triggered a tropical exodus that profoundly altered the complexion of pelagic calcifying communities across the low latitudes (42, 44, 45). Our results thus highlight the sensitivity of tropical planktic foraminifer communities to the synergistic environmental stressors of extreme temperatures, ocean acidification, and deoxygenation at low latitudes during the PETM. Moreover, isotopic filtering could be readily extended to other abrupt events marked by rapid geochemical excursions recorded by marine biocalcifiers (e.g., other Eocene hyperthermal events, abrupt deglaciations) or terrestrial microfossils (e.g., pollen assemblages).

Planktic foraminifer communities have endured for nearly 170 million y and proven resilient in the face of past carbon cycle perturbations and episodes of ocean warming (74). Yet the rapidity of anthropogenic carbon emissions, which is ~10 times faster than carbon emission rates during the PETM (75), will strain their adaptability to future environmental change. Continuing on the current emissions pathway without major policy interventions (SSP3-7.0) will result in a global temperature increase of ~4 °C by the end of the century (1), while a similar magnitude of temperature change occurred over several millennia during the PETM (11–13, 45). Moreover, foraminifer boron isotope records indicate that surface-ocean pH dropped by ~0.3 units during the PETM (15), whereas surface-ocean pH has already dropped by 0.1 units since preindustrial times and global ocean pH is projected to drop by an additional 0.3 to 0.4 pH units by the end of this century (76). Similarly, oxygen concentrations in the global ocean are projected to decrease by an additional 1 to 7% percent by the year 2100, beyond the 2% decrease observed since 1960 (77, 78). In short, the Anthropocene may pose the gravest threat to these prominent marine calcifiers since their near extermination by a cataclysmic asteroid impact some 66 million y ago (79).

Materials and Methods

ODP Site 865 is located at intermediate water depths (~1,510 m) atop Allison Guyot (18°26′N, 179°33′W) in the Mid-Pacific Mountains (31). Benthic foraminifer assemblages suggest a midbathyal (~1,300 m) setting during the late Paleocene (32), and $\delta^{13}C$ records show that PETM records were recovered from holes 865B and 865C (32). Both PETM sections are part of a pelagic cap composed of pure calcareous foraminifer–nannofossil ooze deposited atop Allison Guyot (31). For correlative purposes, bulk-carbonate isotopic analyses ($\delta^{13}C_{bulk}$) were performed on a series of samples taken across both PETM records (Datasets S1 and S2). The two $\delta^{13}C_{bulk}$ records feature comparable CIE magnitudes (~1.5 to 2.0‰) and similar degrees of stratigraphic separation (~10 to 12 cm) between the CIE onset and minimum (Fig. 1 C and D). Accordingly, the CIE onset and minimum in the $\delta^{13}C_{bulk}$ records delimit the main body of the isotopic excursion and served as chronostratigraphic tie points, with intervening samples in the two sections being cross-correlated via linear interpolation assuming a constant sedimentation rate (*SI Appendix*, Table S1). The upper part of the 865B record falls within a coring gap, thus the gradual return to higher values (CIE recovery) seen in the 865C $\delta^{13}C_{bulk}$ record is missing from the 865B record. Biostratigraphic correlation is based on the combined relative abundance of the excursion marker taxa (*A. sibaiyaensis*, *A. africana*, *M. allisonensis*), as determined from assemblage counts (>300 specimens per sample) carried out on the 865B planktic foraminifer assemblages using the same size fraction (>125 μm) employed by earlier studies (27, 30) to delineate taxonomic change in the 865C PETM record (Dataset S4). The two biostratigraphic records (>125 μm) are in good agreement, showing correlative abundance acmes for the excursion taxa (Fig. 1 *E* and *F*).

Foraminifer shells were gleaned from the calcareous ooze by soaking each bulk-sediment sample in a pH-buffered sodium hexametaphosphate hydrogen peroxide (30%v) solution and wet sieving the disaggregated sediment. Resulting coarse fraction (>63 μm) residues were rinsed with distilled water

and oven dried (30 °C) overnight. Specimens used for single-shell stable isotope analyses were handpicked from the >250-μm sieve size fraction of the 865C samples (Dataset S3). Single-shell $\delta^{13}C$ analyses ($n = 548$) were limited to the nine most abundant taxa to ensure statistically robust estimates of reworking in each taxon. Taxonomic coverage of previously published single-shell $\delta^{13}C$ datasets (27, 30) was updated and expanded by including four additional taxa (*A. esnaensis*, *A. esnehensis*, *M. aequa/subbotinae*, and *M. acuta*), generating a new single-shell $\delta^{13}C$ dataset for *A. soldadoensis*, and analyzing additional *Subbotina* spp. specimens. Isotope analyses conducted for this study ($n = 313$), in combination with published single-shell $\delta^{13}C$ data ($n = 235$) from the same samples (27, 30), provided an average of ∼12 values per taxon per stratigraphic sample. All stable isotope measurements (Datasets S1–S3) were performed at the University of California, Santa Cruz Stable Isotope Laboratory using a ThermoScientific Kiel IV carbonate device interfaced with a ThermoScientific MAT 253 dual-inlet gas-source isotope ratio mass spectrometer. External analytical precision for $\delta^{13}C$ on this instrument, as determined by replicate analyses of the calcite standard Carrera Marble, was ≤0.1‰ (±2 SD).

Standard point-counting methods (>300 specimens per sample) were used to compile census data on the nine study taxa (>250 μm) in the 865B PETM section (Dataset S5). Major taxa include *A. sibaiyaensis*, *A. esnehensis*, *A. esnaensis*, *A. soldadoensis*, *M. allisonensis*, *M. acuta*, *M. aequa/subbotinae*, *M. velascoensis*, and *Subbotina* spp. (*SI Appendix*, Fig. S2). The new abundance tallies for each taxon were isotopically filtered (corrected) by subtracting the proportion of reworked specimens indicated by their corresponding single-shell $\delta^{13}C$ values from the 865C section. CIs (95%) on the proportions of reworked specimens were determined via nonparametric bootstrapping (Fig. 3) using the R package *mosaic* (version 1.8.3). The $\delta^{13}C$ values of a taxon in a given sample were randomly resampled (1,000 iterations) and the SEs of the bootstrapped distributions computed (*SI Appendix*, Table S2). R code used for calculating proportions of reworked specimens and bootstrapped error estimates is provided in the supporting information. The few specimens ($n = 3$ of 548) showing intermediate $\delta^{13}C$ values (between +2.0 and +3‰) were not used for isotopic filtering (i.e., they were not included in the per-species, per-sample estimates of the proportion of reworked and in situ taxa). All geochemical and micropaleontological data generated by this study (Datasets S1–S5) will be archived and made available via the National Oceanic and Atmospheric Administration National Center for Environmental Information Paleoclimatology database upon acceptance of the manuscript.

Data Availability. All study data are included in the article and/or supporting information.

ACKNOWLEDGMENTS. Funding and support for this work was provided through the Cushman Foundation for Foraminiferal Research Inc. Johanna M. Resig Dissertator Fellowship and the Geological Society of America Student Research Grants awarded to B.N.H.

1. Z. Hausfather, G. P. Peters, Emissions - The 'business as usual' story is misleading. *Nature* **577**, 618–620 (2020).
2. J. E. Tierney *et al.*, Past climates inform our future. *Science* **370**, eaay3701 (2020).
3. K. Caldeira, M. E. Wickett, Oceanography: Anthropogenic carbon and ocean pH. *Nature* **425**, 365 (2003).
4. R. E. Zeebe, J. C. Zachos, K. Caldeira, T. Tyrrell, Oceans. Carbon emissions and acidification. *Science* **321**, 51–52 (2008).
5. S. C. Doney, V. J. Fabry, R. A. Feely, J. A. Kleypas, Ocean acidification: The other CO_2 problem. *Annu. Rev. Mar. Sci.* **1**, 169–192 (2009).
6. K. J. Kroeker *et al.*, Impacts of ocean acidification on marine organisms: Quantifying sensitivities and interaction with warming. *Glob. Change Biol.* **19**, 1884–1896 (2013).
7. U. Riebesell *et al.*, Reduced calcification of marine plankton in response to increased atmospheric CO_2. *Nature* **407**, 364–367 (2000).
8. R. A. Feely *et al.*, Impact of anthropogenic CO_2 on the $CaCO_3$ system in the oceans. *Science* **305**, 362–366 (2004).
9. L. Fox, S. Stukins, T. Hill, C. G. Miller, Quantifying the effect of anthropogenic climate change on calcifying plankton. *Sci. Rep.* **10**, 1620 (2020).
10. R. P. Speijer, C. Scheibner, P. Stassen, A. M. M. Morsi, Response of marine ecosystems to deep-time global warming: A synthesis of biotic patterns across the Paleocene-Eocene thermal maximum (PETM). *Aust. J. Earth Sci.* **105**, 6–16 (2012).
11. S. Kirtland Turner, P. M. Hull, L. R. Kump, A. Ridgwell, A probabilistic assessment of the rapidity of PETM onset. *Nat. Commun.* **8**, 353 (2017).
12. T. Dunkley Jones *et al.*, Climate model and proxy data constraints on ocean warming across the Paleocene-Eocene thermal maximum. *Earth Sci. Rev.* **125**, 123–145 (2013).
13. G. N. Inglis *et al.*, Global mean surface temperature and climate sensitivity of the early Eocene Climatic Optimum (EECO), Paleocene-Eocene thermal maximum (PETM), and latest Paleocene. *Clim. Past* **16**, 1953–1968 (2020).
14. J. C. Zachos *et al.*, Rapid acidification of the ocean during the Paleocene-Eocene thermal maximum. *Science* **308**, 1611–1615 (2005).
15. D. E. Penman, B. Hönisch, R. E. Zeebe, E. Thomas, J. C. Zachos, Rapid and sustained surface ocean acidification during the Paleocene-Eocene thermal maximum. *Paleoceanography* **29**, 357–369 (2014).
16. M. Gutjahr *et al.*, Very large release of mostly volcanic carbon during the Palaeocene-Eocene thermal maximum. *Nature* **548**, 573–577 (2017).
17. J. P. Kennett, L. D. Stott, Abrupt deep-sea warming, palaeoceanographic changes and benthic extinctions at the end of the Palaeocene. *Nature* **353**, 225–229 (1991).
18. P. L. Koch, J. C. Zachos, P. D. Gingerich, Correlation between isotope records in marine and continental carbon reservoirs near the Palaeocene/Eocene boundary. *Nature* **358**, 319–322 (1992).
19. G. R. Dickens, J. R. O'Neil, D. K. Rea, R. M. Owen, Dissociation of oceanic methane hydrate as a cause of the carbon isotope excursion at the end of the Paleocene. *Paleoceanography* **10**, 965–971 (1995).
20. F. A. McInerney, S. L. Wing, The Paleocene-Eocene thermal maximum: A perturbation of carbon cycle, climate, and biosphere with implications for the future. *Annu. Rev. Earth Planet. Sci.* **39**, 489–516 (2011).
21. L. L. Haynes, B. Hönisch, The seawater carbon inventory at the Paleocene-Eocene thermal maximum. *Proc. Natl. Acad. Sci. U.S.A.* **117**, 24088–24095 (2020).
22. R. Kozdon, D. C. Kelly, J. W. Valley, Diagenetic attenuation of carbon isotope excursion recorded by planktic foraminifers during the Paleocene-Eocene thermal maximum. *Paleoceanogr. Paleoclimatol.* **33**, 367–380 (2018).
23. B. Hupp, D. C. Kelly, Delays, discrepancies, and distortions: Size-dependent sediment mixing and the deep-sea record of the Paleocene-Eocene thermal maximum from ODP site 690 (Weddell Sea). *Paleoceanogr. Paleoclimatol.* **35**, 1–19 (2020).
24. W. H. Berger, G. R. Heath, Vertical mixing in pelagic sediments. *J. Mar. Res.* **26**, 134–143 (1968).
25. W. Schott, "Rate of sedimentation of recent deep-sea sediments" in *Recent Marine Sediments*, P. D. Trask, Ed. (George Banta Publishing, 1955), pp. 409–415.
26. U. Röhl, T. Westerhold, T. J. Bralower, J. C. Zachos, On the duration of the Paleocene-Eocene thermal maximum (PETM). *Geochemistry, Geophys. Geosystems* **8** (2007).
27. D. C. Kelly *et al.*, Rapid diversification of planktonic foraminifera in the tropical Pacific (ODP Site 865) during the Late Paleocene thermal maximum. *Geology* **24**, 423 (1996).
28. D. J. Thomas, J. C. Zachos, T. J. Bralower, E. Thomas, S. Bohaty, Warming the fuel for the fire: Evidence for the thermal dissociation of methane hydrate during the Paleocene-Eocene thermal maximum. *Geology* **30**, 1067–1070 (2002).
29. J. C. Zachos *et al.*, The Palaeocene-Eocene carbon isotope excursion: Constraints from individual shell planktonic foraminifer records. *Philos. Trans.- Royal Soc., Math. Phys. Eng. Sci.* **365**, 1829–1842 (2007).
30. D. C. Kelly, T. J. Bralower, J. C. Zachos, Evolutionary consequences of the latest Paleocene thermal maximum for tropical planktonic foraminifera. *Palaeogeogr. Palaeoclimatol. Palaeoecol.* **141**, 139–161 (1998).
31. W. W. Sager *et al.*, "Site 865" in *Proceedings of the Ocean Drilling Program* (Initial Reports 143, Ocean Drilling Program, College Station, TX), pp. 111–180.
32. T. J. Bralower *et al.*, Late Paleocene to Eocene paleoceanography of the equatorial Pacific Ocean: Stable isotopes recorded at Ocean Drilling Program Site 865, Allison Guyot. *Paleoceanography* **10**, 841–865 (1995).
33. N. J. Shackleton, R. M. Corfield, M. A. Hall, Stable isotope data and the ontogeny of Paleocene planktonic foraminifera. *J. Foraminiferal Res.* **15**, 321–336 (1985).
34. R. D. Norris, Symbiosis as an evolutionary innovation in the radiation of Paleocene planktic foraminifera. *Paleobiology* **22**, 461–480 (1996).
35. M. R. Petrizzo, G. Leoni, R. P. Speijer, B. De Bernardi, F. Felletti, Dissolution susceptibility of some Paleogene planktonic foraminifera from ODP site 1209 (Shatsky rise, Pacific Ocean). *J. Foraminiferal Res.* **38**, 357–371 (2008).
36. R. Kozdon *et al.*, In situ $\delta^{18}O$ and Mg/Ca analyses of diagenetic and planktic foraminiferal calcite preserved in a deep-sea record of the Paleocene-Eocene thermal maximum. *Paleoceanography* **28**, 517–528 (2013).
37. P. B. Wignall, M. J. Benton, Lazarus taxa and fossil abundance at times of biotic crisis. *J. Geol. Soc. London* **159**, 453–456 (1999).
38. R. E. Zeebe, J. C. Zachos, G. R. Dickens, Carbon dioxide forcing alone insufficient to explain Palaeocene-Eocene thermal maximum warming. *Nat. Geosci.* **2**, 576–580 (2009).
39. T. M. P. Nguyen, M. R. Petrizzo, R. P. Speijer, Experimental dissolution of a fossil foraminiferal assemblage (Paleocene-Eocene thermal maximum, Dababiya, Egypt): Implications for paleoenvironmental reconstructions. *Mar. Micropaleontol.* **73**, 241–258 (2009).
40. D. C. Kelly, Response of Antarctic (ODP Site 690) planktonic foraminifera to the Paleocene-Eocene thermal maximum: Faunal evidence for ocean/climate change. *Paleoceanography* **17**, 23-1-23–13 (2002).
41. A. Fredston *et al.*, Range edges of North American marine species are tracking temperature over decades. *Glob. Change Biol.* **27**, 3145–3156 (2021).
42. S. J. Gibbs *et al.*, Ocean warming, not acidification, controlled coccolithophore response during past greenhouse climate change. *Geology* **44**, 59–62 (2016).
43. S. L. Wing *et al.*, Transient floral change and rapid global warming at the Paleocene-Eocene boundary. *Science* **310**, 993–996 (2005).
44. T. Aze *et al.*, Extreme warming of tropical waters during the Paleocene-Eocene thermal maximum. *Geology* **42**, 739–742 (2014).

45. J. Frieling *et al.*, Extreme warmth and heat-stressed plankton in the tropics during the Paleocene-Eocene thermal maximum. *Sci. Adv.* **3**, e1600891 (2017).
46. R. Kozdon, D. C. Kelly, N. T. Kita, J. H. Fournelle, J. W. Valley, Planktonic foraminiferal oxygen isotope analysis by ion microprobe technique suggests warm tropical sea surface temperatures during the Early Paleogene. *Paleoceanography* **26**, PA3206 (2011).
47. E. Thomas, Cenozoic mass extinctions in the deep sea: What perturbs the largest habitat on Earth? *Spec. Pap. Geol. Soc. Am.* **424**, 1–23 (2007).
48. I. Raffi, J. Backman, J. C. Zachos, A. Sluijs, The response of calcareous nannofossil assemblages to the Paleocene Eocene thermal maximum at the Walvis Ridge in the South Atlantic. *Mar. Micropaleontol.* **70**, 201–212 (2009).
49. C. Agnini *et al.*, Responses of calcareous nannofossil assemblages, mineralogy and geochemistry to the environmental perturbations across the Paleocene/Eocene boundary in the Venetian Pre-Alps. *Mar. Micropaleontol.* **63**, 19–38 (2007).
50. I. Raffi, B. De Bernardi, Response of calcareous nannofossils to the Paleocene-Eocene thermal maximum: Observations on composition, preservation and calcification in sediments from ODP Site 1263 (Walvis Ridge - SW Atlantic). *Mar. Micropaleontol.* **69**, 119–138 (2008).
51. T. J. Bralower, J. M. Self-Trail, Nannoplankton malformation during the Paleocene-Eocene thermal maximum and its paleoecological and paleoceanographic significance. *Paleoceanography* **31**, 1423–1439 (2016).
52. C. V. Davis *et al.*, Ocean acidification compromises a planktic calcifier with implications for global carbon cycling. *Sci. Rep.* **7**, 2225 (2017).
53. A. D. Moy, W. R. Howard, S. G. Bray, T. W. Trull, Reduced calcification in modern Southern Ocean planktonic foraminifera. *Nat. Geosci.* **2**, 276–280 (2009).
54. H. De Moel *et al.*, Planktic foraminiferal shell thinning in the Arabian Sea due to anthropogenic ocean acidification? *Biogeosciences* **6**, 1917–1925 (2009).
55. E. B. Osborne, R. C. Thunell, N. Gruber, R. A. Feely, C. R. Benitez-Nelson, Decadal variability in twentieth-century ocean acidification in the California Current Ecosystem. *Nat. Geosci.* **13**, 43–49 (2020).
56. S. A. O'Dea *et al.*, Coccolithophore calcification response to past ocean acidification and climate change. *Nat. Commun.* **5**, 5363 (2014).
57. W. Si, M. P. Aubry, Vital effects and ecologic adaptation of photosymbiont-bearing planktonic foraminifera during the Paleocene-Eocene thermal maximum, implications for paleoclimate. *Paleoceanogr. Paleoclimatol.* **33**, 112–125 (2018).
58. J. O. Shaw *et al.*, Photosymbiosis in planktonic foraminifera across the Paleocene-Eocene thermal maximum. *Paleobiology* **47**, 632–647 (2021).
59. H. J. Spero, D. W. Lea, Intraspecific stable isotope variability in the planktic foraminifera *Globigerinoides sacculifer*: Results from laboratory experiments. *Mar. Micropaleontol.* **22**, 221–234 (1993).
60. S. D'Hondt, J. C. Zachos, G. Schultz, Stable isotopic signals and photosymbiosis in Late Paleocene planktic foraminifera. *Paleobiology* **20**, 391–406 (1994).
61. E. Thomas, N. J. Shackleton, "The Paleocene-Eocene benthic foraminiferal extinction and stable isotope anomalies" in *Correlation of Early Paleogene in Northwest Europe*, R. W. O'B. Knox, R. M. Corfield, R. E. Dunay, Eds. (Geological Society, 1996), pp. 401–441.
62. R. P. Speijer, G. J. Van Der Zwaan, B. Schmitz, The impact of Paleocene/Eocene boundary events on middle neritic benthic foraminiferal assemblages from Egypt. *Mar. Micropaleontol.* **28**, 99–132 (1996).
63. K. Takeda, K. Kaiho, Faunal turnovers in central Pacific benthic foraminifera during the Paleocene-Eocene thermal maximum. *Palaeogeogr. Palaeoclimatol. Palaeoecol.* **251**, 175–197 (2007).
64. M. J. Nicolo, G. R. Dickens, C. J. Hollis, South Pacific intermediate water oxygen depletion at the onset of the Paleocene-Eocene thermal maximum as depicted in New Zealand margin sections. *Paleoceanography* **25**, 1–12 (2010).
65. A. M. E. Winguth, E. Thomas, C. Winguth, Global decline in ocean ventilation, oxygenation, and productivity during the Paleocene-Eocene thermal maximum: Implications for the benthic extinction. *Geology* **40**, 263–266 (2012).
66. X. Zhou, E. Thomas, R. E. M. Rickaby, A. M. E. Winguth, Z. Lu, I/Ca evidence for upper ocean deoxygenation during the PETM. *Paleoceanography* **29**, 964–975 (2014).
67. C. Pälike, M. L. Delaney, J. C. Zachos, Deep-sea redox across the Paleocene-Eocene thermal maximum. *Geochem. Geophys. Geosyst.* **15**, 1038–1053 (2014).
68. S. R. C. Remmelzwaal *et al.*, Investigating ocean deoxygenation during the PETM through the Cr isotopic signature of foraminifera. *Paleoceanogr. Paleoclimatol.* **34**, 917–929 (2019).
69. A. Sluijs *et al.*, Warming, euxinia and sea level rise during the Paleocene-Eocene thermal maximum on the gulf coastal plain: Implications for ocean oxygenation and nutrient cycling. *Clim. Past* **10**, 1421–1439 (2014).
70. W. Yao, A. Paytan, U. G. Wortmann, Large-scale ocean deoxygenation during the Paleocene-Eocene thermal maximum. *Science* **361**, 804–806 (2018).
71. X. Zhou *et al.*, Expanded oxygen minimum zones during the late Paleocene-early Eocene: Hints from multiproxy comparison and ocean modeling. *Paleoceanography* **31**, 1532–1546 (2016).
72. M. O. Clarkson *et al.*, Upper limits on the extent of seafloor anoxia during the PETM from uranium isotopes. *Nat. Commun.* **12**, 399 (2021).
73. C. M. Lowery, P. R. Bown, A. J. Fraass, P. M. Hull, Ecological response of plankton to environmental change: Thresholds for extinction. *Annu. Rev. Earth Planet. Sci.* **48**, 403–429 (2020).
74. A. J. Fraass, D. C. Kelly, S. E. Peters, Macroevolutionary history of the planktic foraminifera. *Annu. Rev. Earth Planet. Sci.* **43**, 139–166 (2015).
75. R. E. Zeebe, A. Ridgwell, J. C. Zachos, Anthropogenic carbon release rate unprecedented during the past 66 million years. *Nat. Geosci.* **9**, 325–329 (2016).
76. IPCC, *Climate Change 2014: Impacts, Adaptation, and Vulnerability. Part A: Global and Sectoral Aspects. Contribution of Working Group II to the Fifth Assessment Report of the Intergovernmental Panel on Climate Change*, C. B. Field *et al.*, Eds. (Cambridge University Press, Cambridge, United Kingdom and New York, NY, 2014), pp. 1132.
77. S. Schmidtko, L. Stramma, M. Visbeck, Decline in global oceanic oxygen content during the past five decades. *Nature* **542**, 335–339 (2017).
78. D. Breitburg *et al.*, Declining oxygen in the global ocean and coastal waters. *Science* **359**, eaam7240 (2018).
79. L. W. Alvarez, W. Alvarez, F. Asaro, H. V. Michel, Extraterrestrial cause for the Cretaceous-Tertiary extinction: Experiment results and theoretical interpretation. *Science* **208**, 241–271 (1980).